CRYSTAL GROWTH & DESIGN

Article

Cite This: *Cryst. Growth Des.* 2018, 18, 1666−1675

pubs.acs.org/crystal

Epitactic Overgrowths of Calcite ($CaCO_3$) on Anhydrite ($CaSO_4$) Cleavage Surfaces

Iris Cuesta Mayorga,[†,‡] José Manuel Astilleros,[*,†,‡] Lurdes Fernández-Díaz,[†,‡] Juan Morales,[§] Manuel Prieto,[∥] Teresa Roncal-Herrero,[⊥] and Liane G. Benning[#,¶,△]

[†]Departamento de Mineralogía y Petrología, Universidad Complutense de Madrid, C/José Antonio Novais 2, Madrid 28040, Spain

[‡]Instituto de Geociencias (CSIC, UCM), C/José Antonio Novais 2, Madrid 28040, Spain

[§]Instituto de Geología Económica Aplicada, Universidad de Concepción, Casilla 160-C, Concepción, Chile

[∥]Departamento de Geología. Universidad de Oviedo, C/Jesús Arias de Velasco, s/n, Oviedo 33005, Spain

[⊥]School of Chemical and Process Engineering and [△]School of Earth and Environment, University of Leeds, LS2 9JT, Leeds, United Kingdom

[#]GFZ, German Research Center for Geosciences, Potsdam, 14473 Germany

[¶]Department of Earth Sciences, Free University of Berlin, 12249, Berlin, Germany

ABSTRACT: We investigate the crystallographic relationships between calcite crystals overgrown on the three main anhydrite cleavage surfaces, (100), (010), and (001), as a result of the interaction between anhydrite surfaces with carbonate-rich aqueous solutions (0.5 mol/L Na_2CO_3). Scanning electron microscope (SEM) images and energy back scattered diffraction (EBSD) analyses reveal that this interaction always leads to oriented nucleation and growth of calcite crystals, characterized by a parallelism between the calcite $\{10\bar{1}4\}$ faces and the corresponding anhydrite cleavage surface. A high density of oriented calcite crystals was observed on the $(001)_{Anh}$ face, while the calcite crystal density was significantly lower on the $(100)_{Anh}$ and $(010)_{Anh}$ faces. On all investigated anhydrite cleavage surfaces, calcite $\{10\bar{1}4\}$ showed at least two excellent matching orientations, both defined by the parallelism between $\langle\bar{4}41\rangle_{Cal}$ and one of the three crystallographic axes of anhydrite. As a result, two different populations of calcite crystals coexisted on the same substrate. In each population four groups of differently orientated crystals could be distinguished, related by symmetric operators inherent to the anhydrite substrates. The coalescence of these differently oriented crystals leads to the formation of twins. The calcite epitactic overgrowth contains an intrinsic intergranular porosity that makes the passivation of anhydrite crystals very unlikely. This characteristic together with the negative molar volume change involved in the anhydrite carbonation reaction makes anhydrite a material suitable to be used in the design of CO_2 capture strategies.

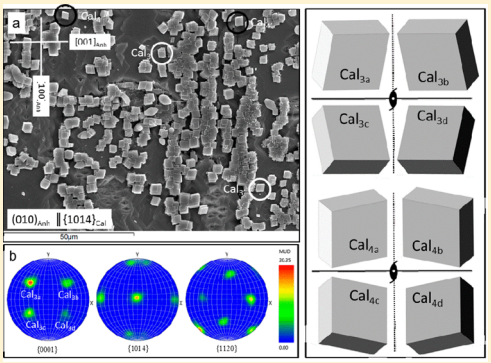

INTRODUCTION

The increasing concern about climate change effects and the overwhelming evidence that connect it to a steady increase in carbon dioxide (CO_2) levels in the atmosphere due to human activities have triggered the search for methods to reduce the volume of industrial carbon dioxide emissions.[1] Some of these methods are inspired by natural processes, which are continuously operating on Earth and which over millions of years have played a major role in regulating atmospheric CO_2 levels.[1] These processes frequently involve the reaction between CO_2-bearing fluids and mineral components released during weathering which can lead to long-lasting CO_2 removal and storage through the precipitation of thermodynamically stable mineral carbonates such as calcite.[2] For example, the efficiency of anthropogenic CO_2 removal through precipitation of $CaCO_3$ phases has been demonstrated through the injection of waters charged with dissolved carbon dioxide of anthropogenic origin into basaltic and peridotitic rocks. Such *in situ* field tests have yielded promising results regarding both the kinetics and the efficiency of the CO_2 removal.[3−5] In a similar fashion, sedimentary evaporitic rocks that make up the huge gypsum ($CaSO_4{\cdot}2H_2O$) and anhydrite ($CaSO_4$) deposits around the world are also highly susceptible for transforming into carbonate minerals upon interaction with water rich in dissolved CO_2. Such sedimentary deposits have been naturally carbonated since Precambrian times, leading to the formation of large volumes of diagenetic limestones in sedimentary basins.[6−9]

In all such systems, in the modern context of CO_2 sequestration through mineral carbonation, the kinetics of the prevalent carbonation reaction is a major concern when assessing the viability and efficiency of CO_2 removal.[10] Mineral

Received: November 20, 2017
Revised: February 7, 2018
Published: February 12, 2018

DOI: 10.1021/acs.cgd.7b01610
Cryst. Growth Des. 2018, 18, 1666−1675

carbonation commonly involves the nucleation of secondary $CaCO_3$ phases on the surface of primary minerals and, for the carbonation reaction to progress, a continuous interaction between the CO_2-bearing fluid phase and the interfaces between primary and secondary phases is required. The reaction progress is strongly controlled by the existence of crystallographic relationships between the original phase and the carbonated end product. This is so because textural overgrowth characteristics that develop on the surface of primary minerals will govern the resulting reaction progress.[11] A direct consequence of this is the slowing down of the kinetics of the reaction. In a recent study we have reported on the carbonation of anhydrite as a result of its interaction with carbonate-rich aqueous solution,[11] and showed how such interactions lead to the complete transformation of single crystals of anhydrite into aggregates of calcite crystals.

It is well-known that the kinetics of anhydrite carbonation is significantly more sluggish than that of gypsum.[11,12] This can partially be explained by the higher reactivity of gypsum surfaces compared to anhydrite surfaces, but also by the existence of epitactic relationships between the calcite overgrowth and the anhydrite substrate, which have not been detected during the carbonation of gypsum under similar conditions.

We hypothesize that the structural elements that enable the development of epitactic relationships between anhydrite and calcite govern the rates and pathways of the carbonation reactions. To assess this, we present here data on the epitatic growth of calcite on the three most common faces in the habit of natural anhydrite crystals: (100), (010), and (001). Our aim is to determine the following: (a) the structural elements that enable the development of epitactic relationships between both phases and (b) the connection between the degree of epitactic fit and those textural characteristics of the calcite overgrowth. A quantitative understanding of the structural factors that control the formation of calcite epitactic overgrowths will enable us to predictively assess the viability of using the carbonation of different calcium-bearing minerals as a means to sequester and store carbon dioxide in a more stable phase as it could be calcite.

1. MATERIALS AND METHODS

We reacted carbonate-rich aqueous solutions with natural, pale blue anhydrite crystals from Naica (Chihuahua, Mexico). Such crystals were freshly cleaved parallel to the (100), (010), and (001) faces using a razor blade prior to each experiment, to obtain fragments with sizes of approximately 3 × 3 × 1 mm^3. In each case, the largest area corresponded to the surface to be studied. We focused our study in these three particular surfaces because they are the most frequent ones in the habit of natural anhydrite crystals[13] and cleavage along them is perfect. The orientation of the sections was determined by observing the interference figures in polarized light microscopy.

Individual anhydrite fragments were placed into glass reactors filled with 5 mL of a commercial 0.5 mol/L Na_2CO_3 solution (pH ≈ 11.4; Fluka) and the reactors were then hermetically sealed. After set periods of time (between 15 min and 4 days), each anhydrite crystal was removed from the solutions and washed with Milli-Q water (resistivity of 18.2 MΩ.cm at 25 °C) to remove any excess salts and rapidly dried using absorbent paper. All experiments were carried out in a thermostatic chamber at 25 ± 0.5 °C and atmospheric pressure. These conditions are within the range of temperatures and pressures which are relevant for the development of anhydrite carbonation processes in Nature.

The morphological and textural characteristics of the initial anhydrite surfaces and of any formed secondary phases resulting from their interaction with the carbonate-rich solution were imaged with a scanning electron microscope (SEM; JEOL JSM 6400, 40 kV). The mineralogy of the formed secondary phases was identified using glancing incidence X-ray diffraction (GIXRD) (PANalytical X'Pert PRO MRD equipped with a Cu Kα X-ray source). Diffraction patterns, collected with a 0.5° incidence to minimize the presence of peaks coming from the bulk of the anhydrite substrate, were matched to files from the ICDD-PDF2 database for anhydrite (00−037−1796) and for the $CaCO_3$ polymorphs calcite (01−071−3699), aragonite (00−001−0628), and vaterite (00−024−0030). Electron backscatter diffraction (EBSD) analyses provided information on crystallographic relationships between the anhydrite substrate and newly formed phase(s). In all the analyses, anhydrite fragments were placed directly on the sample holder without polishing them. EBSD measurements were conducted by means of a ZEISS (EVO 15 MA) SEM equipped with an HKL Nordlys detector (Oxford), using a 17 kV accelerating voltage of the primary beam and a ∼14 mm working distance. The EBSD data were postprocessed using the Aztec (Oxford Instruments) and CHANNEL 5 software. The geometry of the beam-sampler-detector was fixed to a ∼70° tilt. Pole figures obtained from EBSD maps show the degree of co-orientation of the overgrown crystals and the substrate. In all measurements, anhydrite surfaces were oriented prior to setting them in the sampler holder.

CrystalMaker software[14] was used to plot crystal structure projections and to measure repeating periods along different crystallographic directions as well as angles between directions.

2. RESULTS

SEM micrographs of anhydrite (100), (010), and (001) surfaces after interaction with a carbonate-bearing aqueous solution evidence the formation of an overgrowth, which appears as a more or less continuous layer (Figure 1). The degree of coverage of the anhydrite surfaces by the overgrowth increases with time. However, for a given time the degree of coverage varies and depends on the anhydrite surface. In all cases the (001) face always showed the highest degree of coverage. The overgrowths mostly consisted of evenly sized (3−5 μm), euhedral lozenge-shaped microcrystals (Figure 1). In some cases, a few sphere-like aggregates could also be distinguished in the overgrowths formed on anhydrite (010) and (001) surfaces at early stages of reaction (Figure 1c). GIXRD analyses showed that calcite was the main overgrowth component on all anhydrite faces considered, while vaterite was a very minor constituent on the (001) faces. Moreover, although minor vaterite was also observed on the anhydrite (010) surface after a few minutes interaction, this phase was much less abundant than on $(001)_{Anh}$ and was almost absent on $(100)_{Anh}$ regardless the time of interaction.

Thus, we can safely assert that the lozenge-like morphologies correspond to calcite and the sphere-like morphologies correspond to vaterite.[11] According to the angles between faces and edges measured on the SEM micrographs, the habit of calcite crystals is always dominated by the $\{10\bar{1}4\}$ rhombohedron. The calcite crystals grow oriented on the anhydrite substrate, defining an epitactic relationship regardless of the orientation of the substrate. Nevertheless, marked differences in specific epitactic relationships between calcite and the anhydrite (100), (010), and (001) surfaces were observed.

2.1. Calcite Overgrowth on Anhydrite (100) and (010).

The microtopography of anhydrite (100) surfaces is characterized by large and very flat terraces, bounded by macrosteps that run parallel to the [010] and [001] directions (Figure 1a). Post reaction with the carbonate-rich aqueous solution, the anhydrite (100) surfaces developed clear signs of dissolution, in the form of etch pits along [001] (Figure 1a). The orientation

DOI: 10.1021/acs.cgd.7b01610
Cryst. Growth Des. 2018, 18, 1666−1675

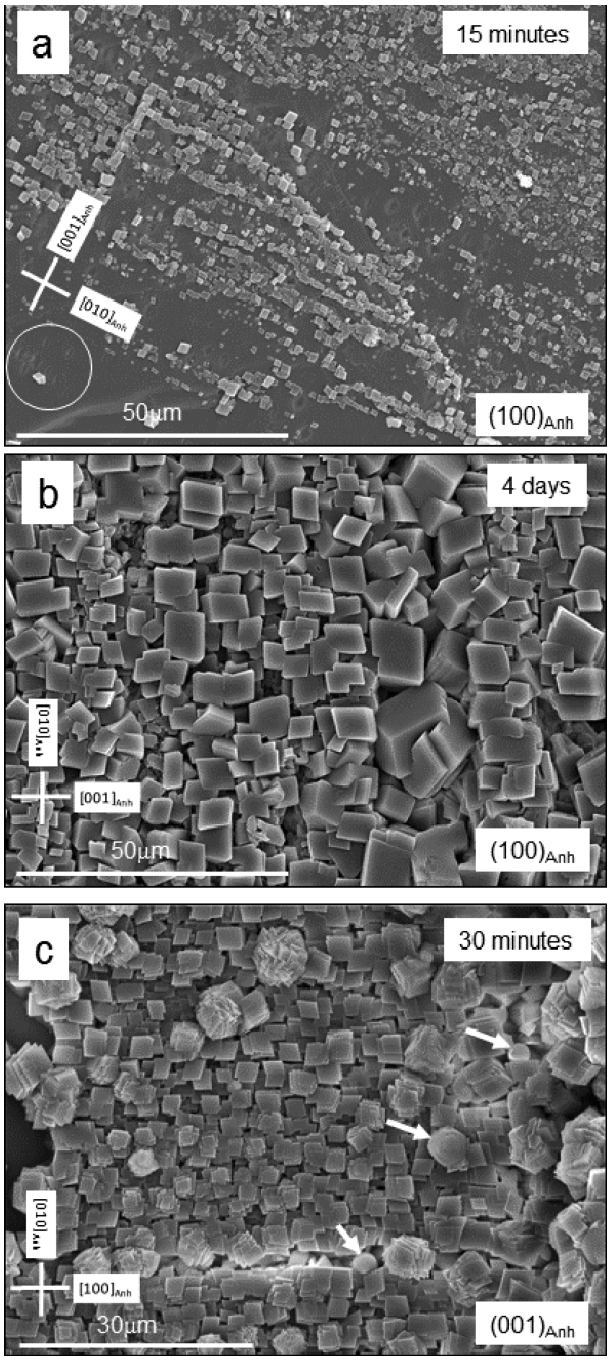

Figure 1. SEM images obtained after 15 min (a), 4 days (b), and 30 min (c) of exposure of anhydrite (100) and (001) surfaces to 0.5 M Na_2CO_3 solutions. The anhydrite surface is covered by a more or less discontinuous layer of small calcite crystals specifically oriented with respect to the substrate. (a) Etch pit orientation (encircled area) enables the identification of the main crystallographic directions on the anhydrite surfaces. (c) Some sphere-like aggregates of vaterite can be distinguished in the overgrowths formed on anhydrite (001) surface (see white arrows).

and morphology of these etch pits helped us confirm the main crystallographic directions. In addition, the dissolution of the surface was accompanied by the growth of new calcite crystals, which formed preferentially on edges and surface defects of the anhydrite (Figure 1a). After 15 min of interaction, around a third of the (100) anhydrite substrate was covered (Figure 1a) by calcite crystals while after 5 h the substrate was fully covered.[11] Such a homogeneous calcite layer on the anhydrite (100) surface after 4 days of reaction (Figure 1b) consists of evenly sized calcite crystals (~5 μm or larger), whose habit is bounded by $\{10\bar{1}4\}$ faces. These calcite crystals appear oriented with respect to the anhydrite substrate in a way that one of the calcite rhombohedron faces is always in contact with the anhydrite (100) plane, defining the epitactic relationship $(100)_{Anh}\|\{10\bar{1}4\}_{Cal}$ (Figure 2a). Moreover, in the majority of these oriented calcite crystals (from here on denoted as Cal_1), one of their $\langle\bar{4}41\rangle_{Cal}$ edges (either $[\bar{4}41]_{Cal}$ or its symmetry-equivalent $[48\bar{1}]$, both resulting from the intersection of the different faces of the $\{10\bar{1}4\}$ form) is oriented parallel to the [001] direction of the anhydrite substrate. A detailed inspection of the micrograph in Figure 2a reveals a second, much less numerous, population of crystals (from here on Cal_2), which are oriented with one of their $\langle\bar{4}41\rangle$ edges parallel to the $[010]_{Anh}$. Consequently, both calcite crystal populations (Cal_1 and Cal_2), are related to each other by a 11.9° rotation about the axis parallel to $[100]_{Anh}$.

The preferential orientations of these calcite crystal overgrowths in relation to the (100) anhydrite cleavage surface was clarified through EBSD analyses (Figure 2b). The pole-orientation density distribution figures (Figure 2a) obtained for the {0001}, $\{10\bar{1}4\}$, and $\{11\bar{2}0\}$ are consistent with the orientation deduced from the SEM photomicrographs for the larger population of calcite crystals (Cal_1). Moreover, EBSD analysis also showed a 4-fold increase in the number of poles, indicating the existence of four symmetry related orientations in Cal_1: Cal_{1a}, Cal_{1b}, Cal_{1c}, and Cal_{1d} (Figure 2c). This increase in the number of poles is the result of the existence of symmetric operators inherent to the anhydrite structure and normal to the (100) substrate plane. These are a twofold screw axis, mirror planes, glide planes, as well as a center of symmetry contained in this plane. Furthermore, the existence of a slight tilt of the pole positions with respect to the expected ones was also noticeable. This is most likely due to a small displacement of the anhydrite crystal in the sample holder during sample preparation for EBSD analyses.

The Cal_2 crystals were far rarer and thus their pole figures are not as clearly recognizable in the EBSD analysis (Figure 2b). However, the slight dispersion around the pole positions could reflect a slight misorientation of the Cal_1 crystals and/or the presence of this smaller population of Cal_2 crystals. This is particularly because the Cal_2 crystals are only slightly rotated (~11.9°) with respect to the major Cal_1 population. Nevertheless, similarly to the Cal_1 crystals, we could define four symmetry related orientations for calcite crystals of the Cal_2 population: Cal_{2a}, Cal_{2b}, Cal_{2c}, and Cal_{2d} (Figure 2d).

Comparing SEM micrographs of different anhydrite surfaces evidence that (010) surfaces showed similar features to (100) surfaces (Figure 3a). Both surfaces were dominated by large and very flat terraces, bounded by macrosteps that ran parallel to [100] and [001] directions. Moreover, calcite crystals formed on such surfaces were also bound by $\{10\bar{1}4\}$ faces and oriented with one of these faces parallel to the anhydrite (010) substrate ($(010)_{Anh}\|\{10\bar{1}4\}_{Cal}$). Furthermore, a majority of calcite crystals had a set of their $\langle\bar{4}41\rangle$ edges oriented parallel to the [001] direction of the anhydrite substrate (Cal_3), while a smaller population had these set of $\langle\bar{4}41\rangle$ edges parallel to the $[100]_{Anh}$ (Cal_4). Pole-orientation density distributions figures obtained by EBSD analyses along the $(010)_{Anh}$/calcite phase boundary again revealed similar features to those obtained for the $(100)_{Anh}$ (Figure 3b). Indeed, the presence of twofold and

DOI: 10.1021/acs.cgd.7b01610
Cryst. Growth Des. 2018, 18, 1666−1675

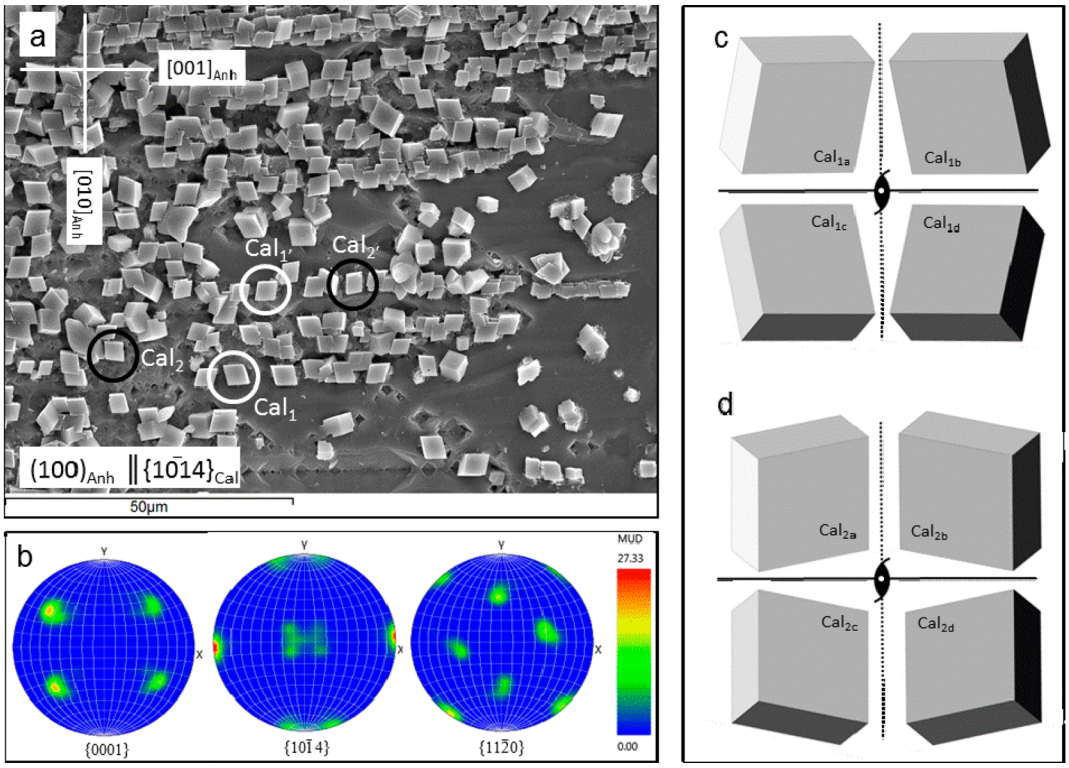

Figure 2. (a) SEM image of calcite crystals grown oriented on the (100) surface of an anhydrite cleaved crystal after 2 h of interaction. The epitaxy involves a matching of the plane (100) of anhydrite with the plane (10$\bar{1}$4) of calcite. The encircled crystals show four different orientations of calcite on the anhydrite substrate which are symmetrically related two by two: Cal_1-Cal_1' and Cal_2-Cal_2' with some of the ⟨$\bar{4}$41⟩ edges running parallel to the $[001]_{Anh}$ and $[010]_{Anh}$, respectively. (b) EBSD pole-orientation density distribution figures which show the crystallographic orientation relationships between the $(100)_{Anh}$ and the overgrown calcite crystals: $(100)_{Anh}\|(10\bar{1}4)_{Cal}$. The number of poles is four times higher than expected reflecting the four alternative orientations shown by the calcite crystals (c) Four alternative orientations, Cal_{1a}, Cal_{1b}, Cal_{1c}, and Cal_{1d}, can be deduced from the pole figures. They reflect the symmetry operators inherent to the anhydrite structure that are normal to the $(100)_{Anh}$ substrate. (c) Four alternative orientations envisaged for the Cal_2 population of crystals.

twofold screw axes, mirror and glide planes, as well as a symmetry center in the anhydrite structure determined the existence of four statistically equivalent orientations of calcite crystals with respect to the anhydrite (010) substrate for each one of the two alternative epitactic relationships defined above.

2.2. Calcite Overgrowth on Anhydrite (001). Anhydrite (001) surfaces were also characterized by flat terraces, bounded by macrosteps that ran parallel to the [100] and [010] directions. Post reaction of these surfaces with the carbonate-rich solutions revealed significantly higher average densities of calcite crystals than on the anhydrite (100) and (010) substrates. The anhydrite (001) substrate was almost completely covered by calcite crystals after 1 h of reaction with the solution.[11] However, at very early stages we observed the development of deep, dissolution-related grooves on the anhydrite (001) substrate, which were oriented parallel to [100] (Figure 4a). This enabled us to define the main crystallographic directions on this surface.[15] Similarly to our observations on both the (100) and (010) surfaces, on the (001) surface calcite crystals with the typical rhombohedron-like habit, bounded by the six faces of the {10$\bar{1}$4} form, are formed. The calcite crystals were oriented with one of their rhombohedron faces parallel to the anhydrite (001) substrate (defining the matching $(001)_{Anh}\|\{10\bar{1}4\}_{Cal}$). Some of these calcite crystals (Cal_5, Figure 4a) are oriented with a set of the ⟨$\bar{4}$41⟩ edges parallel to [100] in the anhydrite substrate. This defines the epitactic relationship $[100]_{Anh}\|\langle\bar{4}41\rangle_{Cal}$. However, a second population of calcite crystals (Cal_6) was slightly tilted (<12°) with respect to those that constitute the Cal_5 population. This tilting occurs in such a way that the ⟨$\bar{4}$41⟩ edges of the calcite run parallel to $[010]_{Anh}$, defining the relationship: $[010]_{Anh}\|\langle\bar{4}41\rangle_{Cal}$. On this (001) anhydrite substrate, the population of Cal_5 crystals was significantly larger than that of Cal_6 crystals. EBSD analyses of the adjacent anhydrite and calcite boundaries also yielded similar crystallographic orientations as those described for the (100) and (010) anhydrite surfaces (Figure 4b).

Finally, we also observed that the nucleation of calcite crystals on the anhydrite substrate with such different and symmetry related orientations often lead to the formation of substrate-induced twins as differently oriented calcite crystals grew and eventually coalesced (Figure 5).

3. DISCUSSION

We demonstrated that the density of calcite crystals formed upon interaction between specific anhydrite surfaces with carbonate-rich aqueous solutions was significantly higher at earlier stages of reaction on $(001)_{Anh}$ compared to on $(100)_{Anh}$ and $(010)_{Anh}$. This is a consequence of the significantly higher reactivity of the $(001)_{Anh}$ surfaces, which dissolves at a much faster rate than both $(100)_{Anh}$ and $(010)_{Anh}$.[16] Consequently, the rate at which Ca^{2+} ions were released from an anhydrite (001) substrate was also faster, resulting in a more rapid increase of local supersaturation in the vicinity of the $(001)_{Anh}$-aqueous solution interface compared to the interface between the aqueous solution and the other two anhydrite cleavage

DOI: 10.1021/acs.cgd.7b01610
Cryst. Growth Des. 2018, 18, 1666−1675

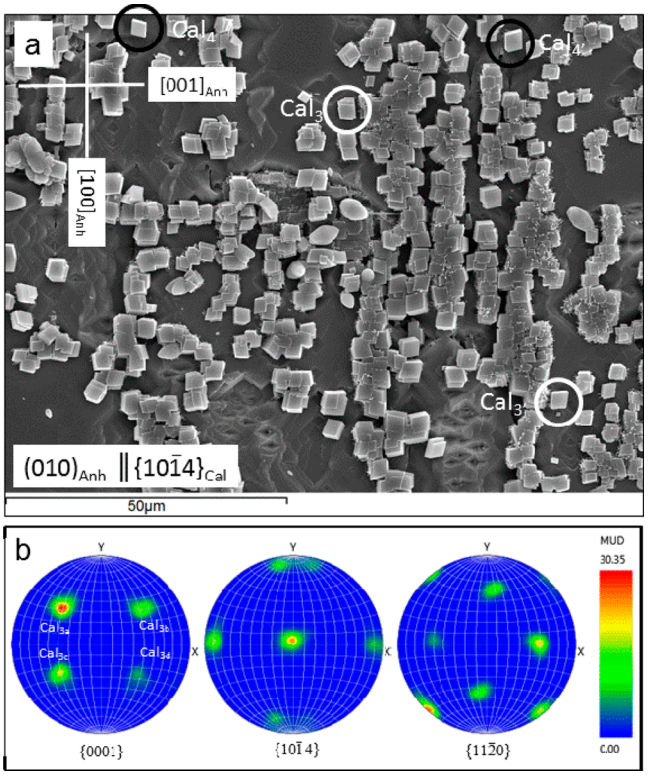

Figure 3. (a) SEM image of calcite crystals grown oriented on the anhydrite (010) surface after 2 h of interaction with the carbonate-rich aqueous solution. The epitaxy is defined by $(100)_{Anh}\|(10\bar{1}4)_{Cal}$. The encircled crystals show the four different orientations of calcite crystals on the anhydrite substrate, which are symmetrically related two by two: Cal_3-Cal_3' and Cal_4-Cal_4'. (b) EBSD pole-orientation density distribution figures. The number of poles is four times higher than expected, reflecting the four alternative orientations shown by the calcite crystals which constitute the Cal_3 population: Cal_{3a}, Cal_{3b}, Cal_{3c}, and Cal_{3d}.

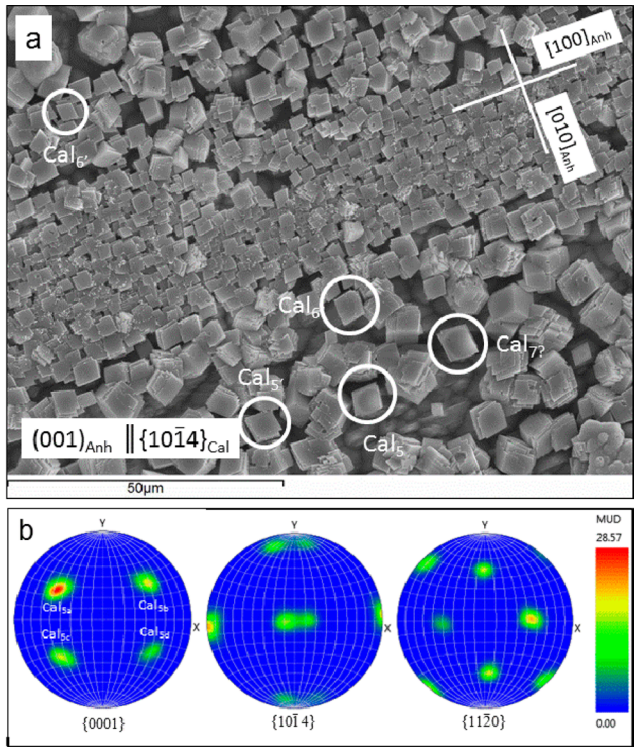

Figure 4. (a) SEM image of calcite crystals grown specifically oriented on the (001) surface of an anhydrite cleavage fragment. The epitaxy involves the matching of the plane (001) of anhydrite with the plane $(10\bar{1}4)$ of calcite. The encircled crystals show alternative orientations of calcite on the anhydrite substrate. The density of the crystals is significantly higher than observed on $(100)_{Anh}$ and on $(010)_{Anh}$ for the same interaction time (2 h). (b) Pole-orientation density distribution figures obtained using EBDS. The number of poles is four times higher than expected, reflecting the four alternative orientations for the Cal_5 population: Cal_{5a}, Cal_{5b}, Cal_{5c}, and Cal_{5d}.

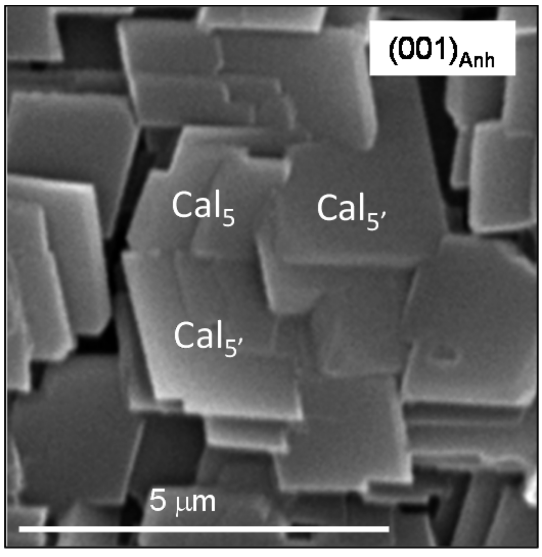

Figure 5. SEM image of substrate-induced calcite twins grown on an anhydrite (001) surface. This type of twins develops when two neighboring, differently oriented calcite crystals (Cal_5 and $Cal_{5'}$) belonging to the same epitactic population (Cal_5) grow to coalesce. The crystal individuals forming the twin are related one to other through a reflection operator belonging to the anhydrite substrate (see Figure 3c).

surfaces, (100) and (010). The nucleation of $CaCO_3$ at higher supersaturation levels can, in turn, explain both, the formation of a higher number of calcite nuclei as well as the formation of a small amount of metastable vaterite at the early stages of the reaction.[11]

Unsurprisingly the habit of all calcite crystals that grew on the three anhydrite surfaces was bounded by the $\{10\bar{1}4\}$ form, that is, the cleavage rhombohedron. This form is the most stable one among the calcite forms because the four different periodic bond chains (PBCs) contained in a $d_{\{10\bar{1}4\}}$ slide provide it with a very strong F character.[17−19] These PBCs run parallel to $[\bar{4}41]$, $[48\bar{1}]$, $[2\bar{2}1]$, and [010] directions in the calcite structure.[20] The two first directions mentioned above are relatively straight chains of carbonate−calcium−carbonate bonds, whereas PBCs parallel to the $[2\bar{2}1]$ and [010] directions consist of undulating bond chains, also composed by carbonate−calcium−carbonate bonds (Figure 6).

Although the development of an epitaxy between an overgrowth and a substrate is not exclusively ruled by geometrical factors, the existence of geometrical similarities between the structures of the involved phases is a requirement for the epitaxy to be possible. These similarities are present in the structures of anhydrite and calcite, despite the fact that both phases crystallize in different crystal systems (anhydrite: space group *Amma*, a = 6.993 Å, b = 6.995 Å, and c = 6.245 Å; calcite: space group $R\bar{3}c$, a = 4.990 Å, and c = 17.061 Å).[21,22] The

DOI: 10.1021/acs.cgd.7b01610
Cryst. Growth Des. 2018, 18, 1666−1675

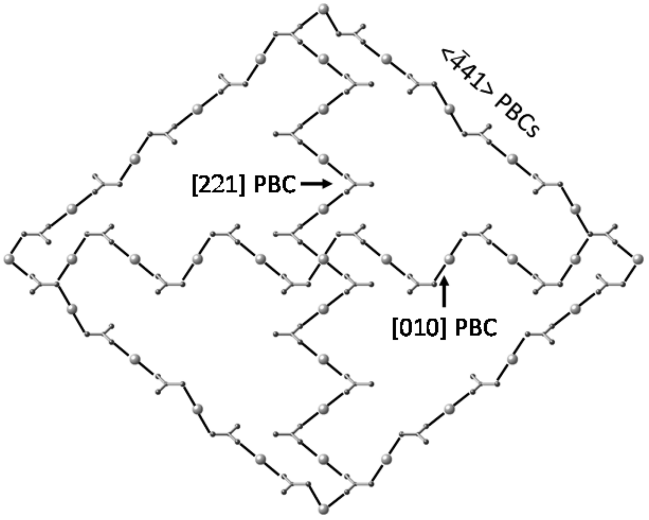

Figure 6. Schematic projection showing the three nonequivalent PBCs contained in the calcite $\{10\bar{1}4\}$ surface. The [221] direction runs parallel to the short diagonal of the rhombus defined by $\langle\bar{4}41\rangle$ directions. The [010] direction runs parallel to the long diagonal. Ca^{2+} cations are depicted by spheres, whereas ball and stick groups represent CO_3^{2-}.

structures of the $\{100\}_{Anh}$, $\{010\}_{Anh}$, and $\{001\}_{Anh}$ surfaces and the $\{10\bar{1}4\}$ form of calcite are based on chains of alternating oxyanion polyhedra and $[n]$-coordinated Ca^{2+}. These chains link to each other, forming layers. In the anhydrite structure three sulfate-calcium-sulfate bond chains can be distinguished.[23] These PBCs run parallel to the crystallographic axes. Consequently, they provide an F-character to the three main anhydrite surfaces since all of them contain two groups of coplanar PBCs. As a result of these crystallographic similarities, the formation of a $\{10\bar{1}4\}$ layer of calcite on any of the three anhydrite surfaces does not interrupt the SO_4−Ca sequence and can ideally continue and match the structure of anhydrite. Indeed, structural continuity "represents the master condition which has to be respected when two crystalline individuals grow within the twinning or epitaxial relationships".[24] Moreover, although the geometries of the sulfate (SO_4^{2-}, tetrahedron) and carbonate (CO_3^{2-}, triangle) oxyanions are different, both are identically charged and have a similar size, which contributes to make possible the development of epitatic relationships between both phases. As a matter of fact, it has been demonstrated that calcite can incorporate small amounts of sulfate substituting carbonate in its bulk structure.[25−29]

Beyond the structural similarities, the formation of the interface between layers of two different phases also requires a good matching of their lattice planes. The mismatch through the interface between the lattices of the two phases involved in the epitaxy can be described by the lattice misfit (mf), which is frequently expressed by means of the equation[30]

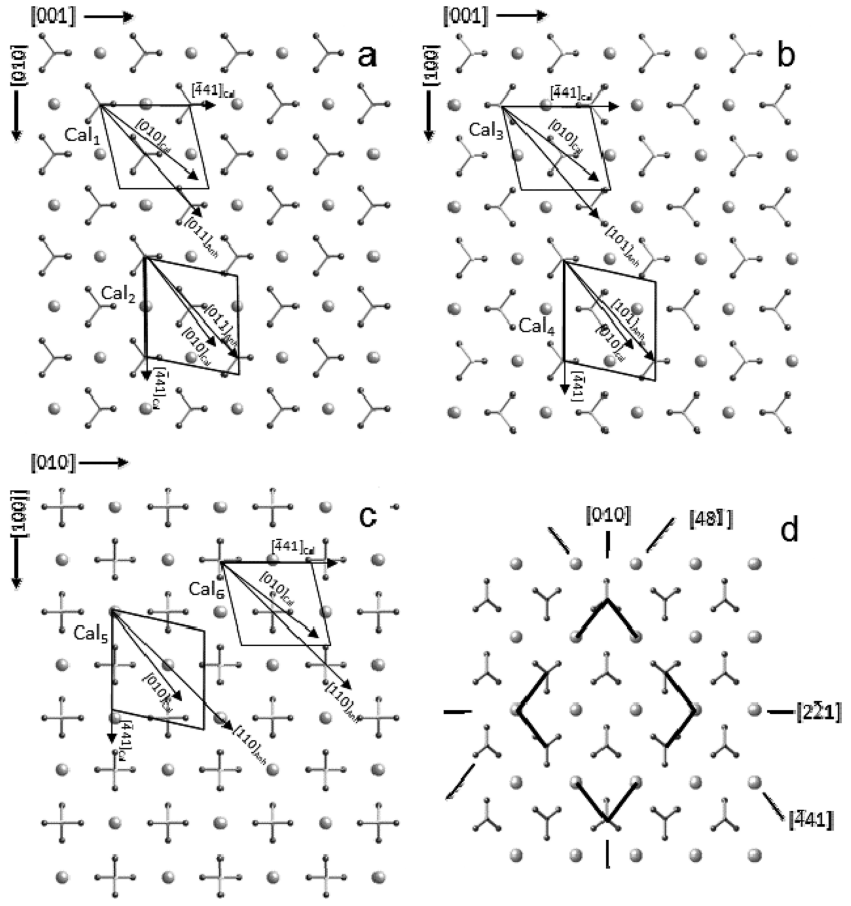

Figure 7. Projections of the crystal structures of a slice of (a) $(200)_{Anh}$, (b) $(020)_{Anh}$, and (c) $(002)_{Anh}$. The superimposed rhombus depicts the $(10\bar{1}4)$ face of the calcite rhombohedron projected in the same orientation as shown in the SEM images. (d) Schematic of the $(10\bar{1}4)_{Cal}$ surface of calcite showing the main directions. Ca^{2+} cations are depicted by spheres, whereas ball and stick groups represent SO_4^{2-} and CO_3^{2-}.

DOI: 10.1021/acs.cgd.7b01610
Cryst. Growth Des. 2018, 18, 1666−1675

Table 1. Epitactic Relationships between Anhydrite ($CaSO_4$) and Calcite ($CaCO_3$)

anhydrite ($CaSO_4$)		Calcite ($CaCO_3$)			misfit (%)	
contact plane	parameter (Å)	contact plane	parameter (Å)	calcite population	linear	angular
(100)	2 × [001] = 12.490	(10$\bar{1}$4)	⟨$\bar{4}$41⟩ = 12.850	1	2.88	–
	⟨011⟩ = 4.689		[010] = 4.990		6.42	∼9.20°
	2 × [010] = 13.990		⟨$\bar{4}$41⟩ = 12.850	2	−8.14	–
	⟨011⟩ = 4.689		[010] = 4.990		6.42	∼2.70°
(010)	2 × [001] = 12.490	(10$\bar{1}$4)	⟨$\bar{4}$41⟩ = 12.850	3	2.88	–
	⟨101⟩ = 9.376		2 × [010] = 9.980		6.44	∼9.20°
	2 × [100] = 13.986		⟨$\bar{4}$41⟩ = 12.850	4	−8.12	–
	⟨101⟩ = 9.376		2 × [010] = 9.980		6.44	∼2.70°
(001)	2 × [100] = 13.986	(10$\bar{1}$4)	⟨$\bar{4}$41⟩ = 12.850	5	−8.12	–
	⟨110⟩ = 9.891		2 × [010] = 9.980		0.90	∼5.50°
	2 × [010] = 13.990		⟨$\bar{4}$41⟩ = 12.850	6	−8.14	–
	⟨110⟩ = 9.891		2 × [010] = 9.980		0.90	∼5.50°
	⟨110⟩ = 9.891		2 × [010] = 9.980	7	0.90	–
	2 × [100] = 13.986		⟨$\bar{4}$41⟩ = 12.850		−8.12	∼5.50°
	2 × [010] = 13.990		⟨$\bar{4}$41⟩ = 12.850		−8.14	∼5.50°

$$mf(\%) = \frac{t_{[uvw]_{Cal}} - t_{[uvw]_{Anh}}}{t_{[uvw]_{Anh}}} \times 100 \quad (1)$$

where $t_{[uvw]}$ is the repeating period along the $[uvw]$ direction of the substrate (anhydrite) and overgrowth (calcite). Negative misfit values mean that the unit cell of the overgrowth is contracted along $[uvw]$ in comparison to the unit cell of the substrate ($t_{[uvw]_{Cal}} < t_{[uvw]_{Anh}}$), whereas a positive misfit value indicates an expansion of the overgrowth unit cell along the same direction. If the difference between the corresponding lattice constants mf is ≤10% to 12%, the lattice matching results in the formation of a coherent substrate−overgrowth interface. This is furthermore, accompanied by the generation of elastic strain and stress and the formation of an epitaxy.[31,32] Figure 7a−d display the projections of the structure of anhydrite on the (100), (010), and (001) planes and calcite on the (10$\bar{1}$4) plane. The superimposed lozenges on the anhydrite structure projections depict a calcite rhombohedron, bounded by ⟨$\bar{4}$41⟩ edges and with one of its (10$\bar{1}$4) faces siting on the projected anhydrite plane. These lozenges are oriented with a pair of their ⟨$\bar{4}$41⟩ edges parallel to a main direction in the anhydrite projection. This matches our observations from the SEM images and EBSD analyses results (Figures 2−4).

As explained above, in most of the calcite crystals (Cal_1 and Cal_3) the epitactic overgrowth of $\{10\bar{1}4\}_{Cal}$ on $(100)_{Anh}$ and $(010)_{Anh}$ was controlled by the parallelism between the $\langle\bar{4}41\rangle_{Cal}$ and $[001]_{Anh}$. For anhydrite, the distance between successive SO_4 groups along [001] is 6.245 Å, i.e., it coincides with the anhydrite c cell parameter. In the calcite structure, the distance between successive equivalent CO_3 groups (repeating period) is 12.850 Å, which is about twice the distance between successive SO_4 groups along $[001]_{Anh}$ (2 × 6.245 Å = 12.49 Å). Similar repeating periods guarantee a good matching between the two structures. Considering a 1:2 ratio between the repeating periods along $[001]_{Anh}$ and $\langle\bar{4}41\rangle_{Cal}$, the misfit is 2.88% (Table 1), which clearly lies within the limits required for epitactic nucleation from solution.[31] Thus, our data show that the excellent matching between both surfaces along these directions explains the development of an oriented overgrowth of calcite on both $(100)_{Anh}$ and $(010)_{Anh}$ surfaces. One additional pair of directions within these contact planes can also be defined in both anhydrite surfaces, $\langle011\rangle_{Anh}\|[010]_{Cal}$ and $\langle101\rangle_{Anh}\|[010]_{Cal}$. These pairs show relatively good matching with linear misfit close to 6.4% (see Table 1). However, an angular divergence between both directions of ∼9.20° does not support the possibility that matching along these directions contribute to the development of the epitaxies.

As we have shown in the SEM images (Figures 2a and 3a), there was a secondary, much less numerous population of calcite crystals, which included two crystal populations (Cal_2 and Cal_4), with one of their $\langle\bar{4}41\rangle_{Cal}$ aligned parallel to the [010] and [100] directions of the $(100)_{Anh}$ and $(010)_{Anh}$ surfaces, respectively. Since the a and b axes in the anhydrite structure are almost identical in length ($b - a$ = 0.002 Å), the linear misfits between the calcite and anhydrite structures along both of these directions are also very similar to ∼8% for both the $[010]_{Anh}\|\langle\bar{4}41\rangle_{Cal}$ and the $[100]_{Anh}\|\langle\bar{4}41\rangle_{Cal}$ alignments. It was also possible to define a second pair of alignments, with $\langle011\rangle_{Anh}\|[010]_{Cal}$ (Cal_2) and $\langle101\rangle_{Anh}\|[010]_{Cal}$ (Cal_4), which were identical to those described for Cal_1 and Cal_3, although with a lower angular divergence (∼2.7°). Although the matches described for Cal_2 and Cal_4 were not as good as those calculated for the Cal_1 and Cal_3 populations, they nevertheless still guarantee the development of an epitactic overgrowth of so oriented calcite crystals on the $(100)_{Anh}$ and $(010)_{Anh}$ surfaces. The good match between the two pair of directions in this second orientation explains, therefore, the development of two nonsymmetrically related populations of calcite crystals rotated by ∼12° with respect to each other. On anhydrite {001} surfaces we have suggested a match between $[100]_{Anh}\|\langle\bar{4}41\rangle_{Cal}$ and $\langle110\rangle_{Anh}\|[010]_{Cal}$ for Cal_5, and $[010]_{Anh}\|\langle\bar{4}41\rangle_{Cal}$ and $\langle110\rangle_{Anh}\|[010]_{Cal}$ for Cal_6 with a slightly better misfits for Cal_5 than Cal_6 (see Table 1). This higher fitting goodness explains the much larger population of Cal_5 crystals.

It is possible to evaluate epitaxy relationship solely on the basis of structural similarities and misfit values. However, as stated by the PBC theory, a minimum interface energy is achieved when, apart from a matching of parallel planes of the substrate and the overgrowth, there is a coincidence between the close-packed atomic rows (defined by the PBCs) contained in these planes.[31] In all the epitactic relationships defined above, the better match involves crystallographic directions parallel to PBCs in both calcite and anhydrite. This factor further favors the development of the oriented overgrowth. Indeed, other alternative epitactic relationships with low misfits

DOI: 10.1021/acs.cgd.7b01610
Cryst. Growth Des. 2018, 18, 1666−1675

values can be envisaged. For instance, the $[110]_{Anh}\|\langle 010\rangle_{Cal}$ alignment on $(001)_{Anh}$ exhibits an excellent match with a linear misfit of 0.90%. However, such an epitaxy is in principle energetically unfavorable with respect to the epitaxies defined above, since the $[110]_{Anh}$ is not parallel to any PBC in the anhydrite structure. Furthermore, although the $[010]_{Cal}$ direction corresponds to a PBC, this is a rough, high-energy, and thus less favorable PBC.[19] In Figure 7c, some crystals could be oriented following this orientation (Cal_7), although this is not clearly supported by SEM observations and EBSD analyses (Table 1).

The existence of epitactic relationships between anhydrite surfaces and calcite overgrowths can influence the kinetics of the carbonation reaction. It has been shown that under certain conditions the development of epitactic overgrowths can lead to *surface passivation*[33] and, as a result, to a slowdown or even full inhibition of any further dissolution−precipitation after the formation of a thin overgrowth. Such overgrowths are often only nanometer-thin, as in the cases of the epitactic overgrowths of otavite ($CdCO_3$) and rhodochrosite ($MnCO_3$) on a calcite {1014} substrate or of hashemite ($BaCrO_4$) on a barite ($BaSO_4$) (001) substrates.[32,34−37] Overgrowths can result from the development of two-dimensional, yet only a few nanometers high, nuclei. These spread rapidly on a substrate and coalesce according to a Frank−van der Merwe or Stranski−Krastanov epitactic growth mechanisms.[32−34] Depending on the goodness of the lattice misfit this commonly involves isostructural phases, which belong to the same mineral group. The formation of this type of overgrowths leads to the almost perfect preservation of the nanotopography of the surface of a substrate.[38,39] A second type of epitactic overgrowth involves the formation on a dissolving substrate of three-dimensional crystals, according to a Volmer−Weber growth mechanism. Commonly, the formation of 3-D crystals takes place when the primary and the secondary phases are non-isostructural but share some structural features and the matching through certain interfaces is good. In this case, even if the overgrowth completely carpets the substrate (like in the case of our calcite crystals growing on the anhydrite surfaces), the armoring is usually imperfect. The existence of hollows, left between differently oriented crystals in the overgrowth, allows a continuous communication between the aqueous solution and the substrate. This way, the progress of the dissolution−crystallization reaction is guaranteed, even if its kinetics is slowed down. Excellent examples of this type of epitaxy are the oriented growth of pharmacolite ($CaHAsO_4{\cdot}2H_2O$) on gypsum and of anglesite ($PbSO_4$) on anhydrite.[40,41] In the latter case, it was demonstrated that the formation of the overgrowth did not prevent the dissolution−precipitation reaction progressing until the complete replacement of anhydrite by anglesite.[42]

The anhydrite−calcite epitaxy described here clearly fits in this latter category. The coalescence of micrometer-sized blocky calcite crystals that are differently oriented on the anhydrite substrates will necessarily lead to the formation of a porous overgrowth. This will, nevertheless, fail to perfectly seal the substrate. The effect of this imperfect sealing is further enhanced by the fact that the replacement of anhydrite by calcite leads to a negative volume change, further contributing to an increase in the porosity of the overgrown calcite layer and explaining that anhydrite crystals in contact with carbonate-bearing solutions can become completely replaced by aggregates of calcite crystals in relatively short times (~15 days under the experimental conditions used in this work).[11]

It is worth highlighting that the existence of two or more equiprobable orientations of the calcite crystals on the anhydrite substrates leads to the development of so-called substrate-induced twinning.[43] The formation of such twins (Figure 5) is a consequence of the coalescence of individuals that are differently oriented with respect to the substrate, but whose orientations are related to each other by symmetry operators inherent to the substrate structure.[42,43] The twin law is, therefore, determined by the substrate symmetry. For instance, in the anhydrite−calcite epitaxy in this current study, individual crystal *a* can be related with individual crystal *d* through a center of symmetry which acts as a twin center (Figure 2c). The formation of substrate-induced twins is a general phenomenon, which has so far been reported to occur during pseudomorphic mineral replacement processes through interface coupled dissolution−crystallization reactions.[42,43]

4. CONCLUSIONS

We evidence here that the epitactic growth of a calcite overgrowth on the three main anhydrite cleavage surfaces, (100), (010), and (001), as a result of their interaction with carbonate-rich aqueous solutions is in all the cases facilitated by (1) the continuity of the anhydrite structure after the deposition of calcite nuclei regardless of substrate type, (2) the goodness of anhydrite-calcite matching through the interface, and (3) the F-character of the anhydrite and calcite surfaces, which guarantees that all crystallographic directions along which both structures show good matchings corresponds to PBCs. Furthermore, we can conclude that moderate goodness of some of the matches defined explain the epitactic growth of calcite on the three anhydrite substrates through a Volmer−Weber mechanism.

Calcite overgrowth consists of micrometric calcite crystals oriented in a number of different ways that produces a certain volume of intergranular porosity within the overgrowth, defined in the contact between differently oriented crystals. This porosity is the consequence of the imperfect assembly between differently oriented rhombohedron-like calcite crystals and is independent of that which will result from the molar volume change involved in the mineral carbonation reaction. Consequently, we can anticipate that, regardless of the molar volume change, mineral carbonation reactions which progress through the formation of micrometer-sized and nonevenly oriented epitactic overgrown crystals are likely to slow down the carbonation due to the progressive thickening of the overgrowth. However, the intrinsic intergranular porosity of this epitactic overgrowth makes unlikely that the transformation will be completely stopped by the overgrowth development. This situation is to be expected when (1) the epitactic overgrowth involves two nonisostructural phases, whose matching through the interface has a moderate goodness, and (2) the primary mineral phase contains symmetry operators normal to the primary-secondary phases interface.

So far, most experimental works were oriented to evaluate the viability of sequestering CO_2 through the carbonation of rock-forming silicate minerals, focusing on olivine and plagioclase.[44,45] In comparison, the carbonation of calcium sulfates, and particularly the carbonation of anhydrite, has significant advantages that render this process as potentially more effective for the capture and long-term storage of CO_2. First, the kinetics of the carbonation reaction is much faster in the case of anhydrite than in the case of olivine and plagioclase. Second, the carbonation of olivine is accompanied by a positive

DOI: 10.1021/acs.cgd.7b01610
Cryst. Growth Des. 2018, 18, 1666−1675

molar volume change, a passivation and self-limiting phenomena which have been reported to take place during the development of this reaction.[46−48] In contrast, anhydrite carbonation is accompanied by a negative molar volume change, which necessarily involves the generation of porosity. Third, the characteristics of calcite epitactic overgrowths, which contain an intrinsic intergranular porosity, irrespective the cleavage surface, that would prevent full passivation during anhydrite carbonation reactions. Finally, in the Earth's surface, anhydrite deposits are widespread and, in general, accessible. Therefore, we conclude that anhydrite carbonation appears as a potentially efficient process worth to be taken into consideration when designing strategies for the capture of CO_2 through solvent mediated mineral replacement reactions.

AUTHOR INFORMATION

Corresponding Author

*E-mail: jmastill@ucm.es. Phone: +34 913944876.

ORCID

José Manuel Astilleros: 0000-0002-4555-6243

Notes

The authors declare no competing financial interest.

ACKNOWLEDGMENTS

This study was supported by the MINECO (Spain) under projects CGL2013-47988-C2-1-P and CGL2016-77138- C2-1-P. I. Cuesta Mayorga acknowledges a FPI (BES-2014-070279) fellowship from the Spanish MINECO and L.G.B. acknowledges financial support from the Helmholtz Recruiting Initiative.

REFERENCES

(1) Oelkers, E. H.; Gislason, S. R.; Matter, J. Mineral Carbonation of CO_2. *Elements* **2008**, *4*, 333−337.

(2) Matter, J. M.; Stute, M.; Snæbjörnsdottir, S.Ó.; Oelkers, E. H.; Gislason, S. R.; Aradottir, E. S.; Sigfusson, B.; Gunnarsson, I.; Sigurdardottir, H.; Gunnlaugsson, E.; Axelsson, G.; Alfredsson, H. A.; Wolff-Boenisch, D.; Mesfin, K.; de la Reguera Taya, D. F.; Hall, J.; Dideriksen, K.; Broecker, W. S. Rapid carbon mineralization for permanent disposal of anthropogenic carbon dioxide emissions. *Science* **2016**, *352*, 1312−1314.

(3) Kelemen, P. B.; Matter, J. In situ carbonation of peridotite for CO_2 storage. *Proc. Natl. Acad. Sci. U. S. A.* **2008**, *105*, 17295−17300.

(4) Matter, J. M.; Kelemen, P. B. Permanent storage of carbon dioxide in geological reservoirs by mineral carbonation. *Nat. Geosci.* **2009**, *2*, 837−841.

(5) Gislason, S. R.; Oelkers, E. H. Carbon storage in basalt. *Science* **2014**, *344*, 373−374.

(6) Kendall, A. C. Late diagenetic calcitization of anhydrite from the Mississippian of Saskatchewan, western Canada. *Sedimentology* **2001**, *48*, 29−55.

(7) Alonso-Zarza, A. M.; Sánchez Moya, Y.; Bustillo Revuelta, M. A.; Sopeña, A.; Delgado Huertas, A. Silicification and dolomitization of anhydrite nodules in argillaceous terrestrial deposits: an example of meteoric-dominated diagenesis from the Triassic of central Spain. *Sedimentology* **2002**, *49*, 303−317.

(8) Warren, J. K. *Evaporites: Sediments, Resources and Hydrocarbons*; Springer: Berlin Heidelberg, 2006; pp 539−542.

(9) Stafford, K. W.; Ulmer-Scholle, D.; Rosales-Lagarde, L. Hypogene calcitization: Evaporite diagenesis in the western Delaware Basin. *Carbonates Evaporites* **2008**, *23*, 89−103.

(10) Ruiz-Agudo, E.; Putnis, C. V.; Putnis, A. Coupled dissolution and precipitation at mineral−fluid interfaces. *Chem. Geol.* **2014**, *383*, 132−146.

(11) Roncal-Herrero, T.; Astilleros, J. M.; Bots, P.; Rodríguez-Blanco, J. D.; Prieto, M.; Benning, L. G.; Fernández-Díaz, L. Reaction pathways and textural aspects of the replacement of anhydrite by calcite at 25° C. *Am. Mineral.* **2017**, *102*, 1270−1278.

(12) Fernández-Díaz, L.; Pina, C. M.; Astilleros, J. M.; Sánchez-Pastor, N. The carbonatation of gypsum: Pathways and pseudomorph formation. *Am. Mineral.* **2009**, *94*, 1223−1234.

(13) Kostov, I.; Kostov, R. I. Crystal habits of minerals. *Bulgarian Academic Monographs (1)*; Pensoft Publishers and Prof. Marin Drinov Academic Publishing House: Sofia, 1999; pp 307−308.

(14) Palmer, D. *CrystalMaker*, v 1.0.4; CrystalMaker Software Ltd: Begbroke, Oxfordshire, England, 2005.

(15) Shindo, H.; Seo, A.; Watabe, T. Structures of the $CaSO_4$ (001) surface studied with atomic force microscopy in air and in solution. *Phys. Chem. Chem. Phys.* **2001**, *3*, 230−234.

(16) Shindo, H.; Igarashi, T.; Karino, W.; Seo, A.; Yamanobe-Hada, M.; Haga, M. Stabilities of crystal faces of anhydrite ($CaSO_4$) compared by AFM observation of facet formation processes in aqueous solutions. *J. Cryst. Growth* **2010**, *312*, 573−579.

(17) Hartman, P.; Perdok, W. On the relations between structure and morphology of crystals. I. *Acta Crystallogr.* **1955**, *8*, 49−52.

(18) Paquette, J.; Reeder, R. Relationship between surface structure, growth mechanism, and trace element incorporation in calcite. *Geochim. Cosmochim. Acta* **1995**, *59*, 735−749.

(19) Aquilano, D.; Bruno, M.; Massaro, F. R.; Rubbo, M. Theoretical equilibrium shape of calcite. 2. [441] zone and its role in biomineralization. *Cryst. Growth Des.* **2011**, *11*, 3985−3993.

(20) Heijnen, W. M. M. The morphology of gel grown calcite. *Neues Jahrb. Mineral., Monatsh.* **1985**, *8*, 357−371.

(21) Hawthorne, F. C.; Ferguson, R. B. Anhydrous sulphates. II. Refinement of the crystal structure of anhydrite. *Can. Mineral.* **1975**, *13*, 289−292.

(22) Effenberger, H.; Mereiter, K.; Zemann, J. Crystal structure refinements of magnesite, calcite, rhodochrosite, siderite, smithonite, and dolomite, with discussion of some aspects of the stereochemistry of calcite type carbonates. *Z. Kristallogr. - Cryst. Mater.* **1981**, *156*, 233−243.

(23) Aquilano, D.; Rubbo, M.; Catti, M.; Pavese, A.; Ugliengo, P. Theoretical equilibrium and growth morphology of anhydrite ($CaSO_4$) crystals. *J. Cryst. Growth* **1992**, *125* (3−4), 519−532.

(24) Massaro, F. R.; Pastero, L.; Costa, E.; Sgualdino, G.; Aquilano, D. Single and twinned Li_2CO_3 crystals (zabuyelite) epitaxially grown on {0001} and {1014} forms of $CaCO_3$ (calcite) crystals. *Cryst. Growth Des.* **2008**, *8*, 2041−2046.

(25) Frisia, S.; Borsato, A.; Fairchild, I. J.; Susini, J. Variations in atmospheric sulphate recorded in stalagmites by synchrotron micro-XRF and XANES analyses. *Earth Planet. Sci. Lett.* **2005**, *235*, 729−740.

(26) Arroyo-de Dompablo, M. E.; Fernández-González, M. A.; Fernández-Díaz, L. Computational investigation of the influence of tetrahedral oxoanions (sulphate, selenate and chromate) on the stability of calcium carbonate polymorphs. *RSC Adv.* **2015**, *5*, 59845−59852.

(27) Fernández-Díaz, L.; Fernández-González, A.; Prieto, M. The role of sulfate groups in controlling $CaCO_3$ polymorphism. *Geochim. Cosmochim. Acta* **2010**, *74*, 6064−6076.

(28) Balan, E.; Aufort, J.; Pouillé, S.; Dabos, M.; Blanchard, M.; Lazzeri, M.; Rollion-Bard, C.; Blamart, D. Infrared spectroscopic study of sulfate-bearing calcite from deep-sea bamboo coral. *Eur. J. Mineral.* **2017**, *29*, 397.

(29) Perrin, J.; Rivard, C.; Vielzeuf, D.; Laporte, D.; Fonquernie, C.; Ricolleau, A.; Cotte, M.; Floquet, N. The coordination of sulfur in synthetic and biogenic Mg calcites: The red coral case. *Geochim. Cosmochim. Acta* **2017**, *197*, 226−244.

(30) Van der Merwe, J. H. The role of lattice misfit in epitaxy. *Crit. Rev. Solid State Mater. Sci.* **1978**, *7*, 209−231.

(31) Chernov, A. A. Nucleation and Epitaxy. In *Modern Crystallography III. Crystal Growth*; Springer Series on Solid-State Science 36; Springer-Verlag: Berlin Heidelberg, 1984; pp 48−103.

DOI: 10.1021/acs.cgd.7b01610
Cryst. Growth Des. 2018, 18, 1666−1675

(32) Shtukenberg, A. G.; Astilleros, J. M.; Putnis, A. Nanoscale observations of epitaxial growth of hashemite on Barite (001). *Surf. Sci.* **2005**, *590*, 212−223.
(33) Prieto, M.; Astilleros, J. M.; Fernández-Díaz, L. Environmental remediation by crystallization of solid solutions. *Elements* **2013**, *9*, 195−201.
(34) Pérez-Garrido, C.; Fernández-Díaz, L.; Pina, C. M.; Prieto, M. *Surf. Sci.* **2007**, *601*, 5499−5509.
(35) Pérez-Garrido, C.; Astilleros, J. M.; Fernández-Díaz, L.; Prieto, M. In situ AFM observations of the interaction between calcite (1014) surfaces and Cd-bearing aqueous solutions. *J. Cryst. Growth* **2009**, *311*, 4730−4739.
(36) Godelitsas, A.; Astilleros, J. M. Dissolution, sorption/(re)-precipitation, formation of solid solutions and crystal growth phenomena on mineral surfaces: implications for the removal of toxic metals from the environment. In *Ion partitioning in ambient-temperature aqueous systems*, Prieto, M.; Stoll, H., Eds.; EMU Notes in Mineralogy 10; European Mineralogical Union and the Mineralogical Society of Great Britain and Ireland: London, 2010; pp 289−324.
(37) Riechers, S. L.; Kerisit, S. N. Anisotropic growth of otavite on calcite: Implications for heteroepitaxial growth mechanisms. *Cryst. Growth Des.* **2018**, *18*, 159−170.
(38) Astilleros, J. M.; Pina, C. M.; Fernández-Díaz, L.; Putnis, A. Nanoscale growth of solids crystallising from multicomponent aqueous solutions. *Surf. Sci.* **2003**, *545*, L767.
(39) Astilleros, J. M.; Pina, C. M.; Fernández-Díaz, L.; Prieto, M.; Putnis, A. Nanoscale phenomena during the growth of solid solutions on calcite {1014} surfaces. *Chem. Geol.* **2006**, *225*, 322−335.
(40) Rodríguez-Blanco, J. D.; Jiménez, A.; Prieto, M. Oriented overgrowth of pharmacolite ($CaHAsO_4{\cdot}2H_2O$) on gypsum ($CaSO_4{\cdot}2H_2O$). *Cryst. Growth Des.* **2007**, *7*, 2756−2763.
(41) Morales, J.; Astilleros, J. M.; Fernández-Díaz, L.; Álvarez-Lloret, P.; Jiménez, A. Anglesite ($PbSO_4$) epitactic overgrowths and substrate-induced twinning on anhydrite ($CaSO_4$) cleavage surfaces. *J. Cryst. Growth* **2013**, *380*, 130−137.
(42) Morales, J.; Astilleros, J. M.; Jiménez, A.; Göttlicher, J.; Steininger, R.; Fernández-Díaz, L. Uptake of dissolved lead by anhydrite surfaces. *Appl. Geochem.* **2014**, *40*, 89−96.
(43) Pinto, A. J.; Jiménez, A.; Prieto, M. Interaction of phosphate-bearing solutions with gypsum: Epitaxy and induced twinning of brushite ($CaHPO_4{\cdot}2H_2O$) on the gypsum cleavage surface. *Am. Mineral.* **2009**, *94*, 313−322.
(44) King, H. E.; Plümper, O.; Putnis, A. Effect of secondary phase formation on the carbonation of olivine. *Environ. Sci. Technol.* **2010**, *44*, 6503−6509.
(45) Olajire, A. A. A review of mineral carbonation technology in sequestration of CO_2. *J. Pet. Sci. Eng.* **2013**, *109*, 364−392.
(46) Béarat, H.; McKelvy, M. J.; Chizmeshya, A. V. G.; Gormley, D.; Nunez, R.; Carpenter, R. W.; Squires, K.; Wolf, G. H. Carbon sequestration via aqueous olivine mineral carbonation: Role of passivating layer formation. *Environ. Sci. Technol.* **2006**, *40*, 4802−4808.
(47) Munz, I. A.; Brandvoll, Ø.; Haug, T. A.; Iden, K.; Smeets, R.; Kihle, J.; Johansen, H. Mechanisms and rates of plagioclase carbonation reactions. *Geochim. Cosmochim. Acta* **2012**, *77*, 27−51.
(48) Hövelmann, J.; Austrheim, H.; Jamtveit, B. Microstructure and porosity evolution during experimental carbonation of a natural peridotite. *Chem. Geol.* **2012**, *334*, 254−265.

DOI: 10.1021/acs.cgd.7b01610
Cryst. Growth Des. 2018, 18, 1666−1675